

A linkage of Trefftz method and method of fundamental solutions for annular Green's functions using addition theorem

Shiang-Chih Shieh^{1*}, Ying-Te Lee¹, Shang-Ru Yu¹ and Jeng-Tzong Chen^{1,2}

¹Department of Harbor and River Engineering

National Taiwan Ocean University, Keelung, Taiwan

²Department of Mechanical and Mechatronic Engineering

National Taiwan Ocean University, Keelung, Taiwan

*E-Mail: M96520027@mail.ntou.edu.tw

NSC PROJECT: NSC 97-2221-E-019-015-MY3

ABSTRACT

In this paper, the Green's function for the annular Laplace problem is first derived by using the image method which can be seen as a special case of method of fundamental solutions. Three cases, fixed-fixed, fixed-free and free-fixed boundary conditions are considered. Also, the Trefftz method is employed to derive the Green's function by using T-complete sets. By employing the addition theorem, both solutions are found to be mathematically equivalent when the number of Trefftz bases and the number of image points are both infinite. On the basis of the finite number of degrees of freedom, the convergence rates of both methods are demonstrated and compared with each other. In the successive image process, the final two images freeze at the origin and infinity, where their singularity strengths can be analytically and numerically determined in a consistent manner.

Keywords: Green's function, method of fundamental solutions, image method, Trefftz method

1. INTRODUCTION

Trefftz in 1926 presented the Trefftz method for solving boundary value problems by superimposing the functions satisfying the governing equation, although various versions of the Trefftz method, *e.g.*, direct and indirect formulations have been developed [1]. The unknown coefficients are determined by matching the boundary condition.

In the potential theory, it is well known that the method of fundamental solutions (MFS) can solve potential problems when a fundamental solution is known. This method was proposed by Kupradze and Aleksidze [2] in 1964. Extensive applications in solving a broad range of problems such as acoustics [3] have been investigated. The MFS can be viewed as an indirect boundary element method (BEM) with concentrated sources instead of boundary distributions. The initial idea is to approximate the solution through a linear combination of fundamental solutions with sources

located outside the domain of the problem. Moreover, it has certain advantages over BEM, *e.g.*, no singularity and no boundary integral. However, ill-posed behavior is inherent in the regular formulation. Trefftz method and MFS are both mesh reduction methods.

Green's function has been studied and applied in many fields by mathematicians as well as engineers [4]. Green's functions are useful building blocks for attacking more realistic problems. But only a few of simple regions allow a closed-form Green's function for the Laplace equation. For example, one aperture or circular sector in the half plane, infinite strip, semi strip or infinite wedge can be mapped by elementary analytic functions, making their Green's function expressed in a closed form. A closed-form Green's function for the Laplace equation by using the mapping function becomes impossible for the complicated domain except for some simple cases. For the image method, Thomson [5] proposed the concept of reciprocal radii to find the image source to satisfy the homogeneous Dirichlet boundary condition. Chen and Wu [6] proposed an alternative way to find the location of image through the degenerate kernel. The Green's function of a circular ring has been solved using complex variable by Courant and Hilbert [7]. However, it is limited to extend to three-dimensional space.

Mathematical studies on the MFS have been investigated by some researchers. Bogomolny [8] studied the stability and error bound of MFS. Li *et al.* [9] used the effective condition number to study the collocation approaches of MFS and Trefftz method. They found that the condition number of MFS is much worse than that of the Trefftz method. Although the Trefftz method and MFS have a long history individually, the link between the two methods was not discussed in detail in the literature until the Chen *et al.*'s paper [10]. They proved the equivalence between the Trefftz method and the MFS for the Laplace and biharmonic problems with the circular domain. The keypoint is the use of the degenerate kernel or so-called the addition theorem. They only proved the equivalence by demonstrating a simple circle with angular distribution of singularity to link the two methods. Later, the similar viewpoint was also found

by Schaback [11]. However, Schaback claimed that MFS is closely connected to the Trefftz method but they are not equivalent in the error analysis. He found that the MFS for the source points on the far-away field yields a trial space that belongs to harmonic polynomials. However, an extension study for the equivalence of Trefftz method and MFS for a doubly-connected domain problem is not trivial. This is the main concern of this paper. Here, we put singularities along the radial direction in the method of image in stead of angular distributions. **The Green's function of Laplace equation was by using the image method for simple case in Greenberg [14].**

In this paper, we focus on proving the mathematical equivalence between the Trefftz method and MFS on the Green's function for annular Laplace problems subject to fixed-fixed, fixed-free and free-fixed boundary conditions. By employing the image method and addition theorem, the equivalence of the solution using two methods will be proved when the number of image points and number of the Trefftz bases are infinite. The image method is seen as a special case of MFS, since its image singularities locate outside the domain. The convergence rate on the basis of finite number of degrees of freedoms for the Trefftz method and MFS is also discussed. The final frozen image location in the successive mapping is also examined. Besides, the singularity strength can be analytically and numerically determined. The solution by using the image method also indicates that a free constant is required to be complete for the solution which is always overlooked in the conventional MFS.

2. Derivation of the Green's function for an annular case by using the image method

For a two-dimensional annular problem as shown in Fig. 1, the Green's function satisfies

$$\nabla^2 G(x, \zeta) = \delta(x - \zeta), x \in \Omega, \quad (1)$$

where Ω is the domain of interest and δ denotes the Dirac-delta function for the source at ζ . For simplicity, the Green's function is considered to be subjected to the Dirichlet boundary condition

$$G(x, \zeta) = 0, x \in B_1 \cup B_2, \quad (2)$$

where B_1 and B_2 are the inner and outer boundaries, respectively. We extend a circular case [6] to an annular case. An annular case can be seen as a combination of interior and exterior problems as shown in Fig. 2. As mentioned in [6], the interior and exterior Green's functions can satisfy the homogeneous Dirichlet boundary conditions if the image source is correctly selected. The closed-form Green's functions for both interior and exterior problems are written to be the same form

$$G(x, \zeta) = \ln|x - \zeta| - \ln|x - \zeta'| + \ln a - \ln R_\zeta, x \in \Omega, \quad (3)$$

where a is the radius of the circle, $\zeta = (R_\zeta, 0)$, R_ζ is the distance from the source to the center of the circle, ζ' is the image source and its position is at $(a^2/R_\zeta, 0)$

as shown in Fig. 3.

By matching the homogeneous Dirichlet boundary conditions for the outer and inner boundaries, we introduce the image points ζ_1 and ζ_2 , respectively. Since ζ_2 results in the nonhomogeneous boundary conditions on the outer boundary, we need to introduce an extra image point ζ_3 . Similarly, ζ_1 results in the nonhomogeneous boundary conditions on the inner boundary and an additional image point ζ_4 is also required. Repeating the same procedure, we have a series of image sources locating at

$$\zeta_1 = \frac{b^2}{R_\zeta}, \zeta_3 = \frac{b^2 R_\zeta}{a^2}, \zeta_5 = \frac{b^2}{R_\zeta} \frac{b^2}{a^2}, \zeta_7 = \frac{b^2 R_\zeta}{a^2} \frac{b^2}{a^2}, \quad (4)$$

$$\zeta_{4n-3} = \frac{b^2}{R_\zeta} \left(\frac{b^2}{a^2}\right)^{n-1}, \zeta_{4n-1} = \frac{b^2 R_\zeta}{a^2} \left(\frac{b^2}{a^2}\right)^n, n \in N,$$

$$\zeta_2 = \frac{a^2}{R_\zeta}, \zeta_4 = \frac{a^2 R_\zeta}{b^2}, \zeta_6 = \frac{a^2}{R_\zeta} \frac{a^2}{b^2}, \zeta_8 = \frac{a^2 R_\zeta}{b^2} \frac{a^2}{b^2}, \dots, \quad (5)$$

$$\zeta_{4n-2} = \frac{a^2}{R_\zeta} \left(\frac{a^2}{b^2}\right)^{n-1}, \zeta_{4n} = \frac{a^2 R_\zeta}{b^2} \left(\frac{a^2}{b^2}\right)^{n-1}, n \in N.$$

Fig. 4 and Table 1 depict a series of images for the three annular problems. We consider the fundamental solution $U(s, x)$ for the source singularity at s such that

$$\nabla^2 U(x, s) = 2\pi\delta(x - s). \quad (6)$$

Then, we obtain the fundamental solution as follows:

$$U(x, s) = \ln r, \quad (7)$$

where r is the distance between s and x ($r \equiv |x - s|$).

Based on the separable property of addition theorem or the so-called degenerate kernel, the fundamental solution $U(x, s)$ can be expanded into series form by separating the field point $x(\rho, \phi)$ and source point $s(R, \theta)$ in the polar coordinate [10]:

$$U(s, x) = \begin{cases} U^I(R, \theta, \rho, \phi) = \ln R - \sum_{m=1}^{\infty} \frac{1}{m} \left(\frac{\rho}{R}\right)^m \cos m(\theta - \phi), R \geq \rho, \\ U^E(R, \theta, \rho, \phi) = \ln \rho - \sum_{m=1}^{\infty} \frac{1}{m} \left(\frac{R}{\rho}\right)^m \cos m(\theta - \phi), R < \rho, \end{cases} \quad (8)$$

where the superscripts of I and E denotes the interior and exterior regions, respectively. It is noted that the leading term and the numerator in the above expansion involve the larger argument to ensure the log singularity and the series convergence, respectively. In order to iteratively match the inner and outer homogenous Dirichlet boundary conditions, combination of all the images yields the main part of the solution

$$G_m(x, \zeta) = \frac{1}{2\pi} \left[\ln|x - \zeta| - \sum_{i=1}^N \left(\ln|x - \zeta_{4i-3}| + \ln|x - \zeta_{4i-2}| - \ln|x - \zeta_{4i-1}| - \ln|x - \zeta_{4i}| \right) \right]. \quad (9)$$

2.1 Satisfaction of the boundary condition by using interpolation functions

Although $G_m(x, \zeta)$ is the particular solution of the Green's function, $G_m(x, \zeta)$ in Eq. (9) can not satisfy

both the inner and outer boundary conditions of $G_m(x_a, \zeta) = G_m(x_b, \zeta) = 0$, where $x_a = (a, \phi)$, $x_b = (b, \phi)$, $0 \leq \phi \leq 2\pi$. In order to satisfy both the inner and outer boundary conditions, we introduce

$$G(x, \zeta) = G_m(x, \zeta) - \left(\frac{\ln \rho - \ln a}{\ln b - \ln a}\right)G_m(x_b, \zeta) - \left(\frac{\ln b - \ln \rho}{\ln b - \ln a}\right)G_m(x_a, \zeta), \quad a \leq \rho \leq b, \quad (10)$$

where $\left(\frac{\ln \rho - \ln a}{\ln b - \ln a}\right)$ and $\left(\frac{\ln b - \ln \rho}{\ln b - \ln a}\right)$ are interpolation functions with the Kroneker-delta property. Therefore, Eq. (10) can be rewritten as

$$G(x, \zeta) = \frac{1}{2\pi} \left\{ \ln|x-\zeta| - \sum_{i=1}^N \left[\ln|x-\zeta_{4i-3}| + \ln|x-\zeta_{4i-2}| - \ln|x-\zeta_{4i-1}| - \ln|x-\zeta_{4i}| \right] - \left(\frac{\ln \rho - \ln a}{\ln b - \ln a}\right) \left[\ln b \left(\frac{R_\zeta^2}{a^2}\right)^N - \sum_{m=1}^{\infty} \frac{1}{m} \left[\left(\frac{a^2}{b^2}\right)^N \frac{R_\zeta}{b}\right]^m \cos m(\theta - \phi) \right] - \left(\frac{\ln b - \ln \rho}{\ln b - \ln a}\right) \left[\ln R \left(\frac{R_\zeta^2}{a^2}\right)^N - \sum_{m=1}^{\infty} \frac{1}{m} \left[\left(\frac{a^2}{b^2}\right)^N \frac{a}{R_\zeta}\right]^m \cos m(\theta - \phi) \right] \right\}, \quad (11)$$

after expanding the fundamental solutions of G_m in Eq. (9) by using the addition theorem. As N approaches infinity (*i.e.* many image points), Eq. (11) reduces to

$$G(x, \zeta) = \frac{1}{2\pi} \left[\ln|x-\zeta| - 2N \ln \frac{R_\zeta}{a} - \left(\frac{\ln R_\zeta - \ln a}{\ln b - \ln a}\right) \ln b - \left(\frac{\ln b - \ln R_\zeta}{\ln b - \ln a}\right) \ln \rho \right] - \frac{1}{2\pi} \sum_{i=1}^N \left[\ln|x-\zeta_{4i-3}| + \ln|x-\zeta_{4i-2}| - \ln|x-\zeta_{4i-1}| - \ln|x-\zeta_{4i}| \right], \quad (12)$$

due to $\lim_{N \rightarrow \infty} \left(\frac{a^2}{b^2}\right)^N = 0$ and $\left(\frac{a}{b}\right) < 1$. Eq.(12) indicates that not only image singularities at ζ_{4i-3} , ζ_{4i-2} , ζ_{4i-1} and ζ_{2i} , $i = 1, 2, 3, \dots$, but also one singularity of

$\left(\frac{\ln b - \ln R_\zeta}{\ln b - \ln a}\right) \ln \rho$ at the origin and two rigid body terms

of $2N \ln \frac{R_\zeta}{a}$ and $\left(\frac{\ln R_\zeta - \ln a}{\ln b - \ln a}\right) \ln b$ for the fixed-fixed

case are required. The Green's function in Eq. (12) satisfies the governing equation and boundary conditions at the same time. It is found that a conventional MFS loses a free constant and completeness may be questionable. Similarly, the image method can be extended to solve fixed-free and free-fixed cases. All the series solutions are analytically derived in Table 1 not only for fixed-fixed but also for fixed-free and free-fixed cases.

2.2 Satisfaction of boundary conditions using two singularity strengths at the origin and infinity

After successive image process, the final two image location freeze at the origin and infinity. There are two strength of singularity to be determined. Therefore, Eq.(9) can be rewritten as

$$G(x, \zeta) = \frac{1}{2\pi} \left[\ln|x-\zeta| - \sum_{i=1}^N \left(\ln|x-\zeta_{4i-3}| + \ln|x-\zeta_{4i-2}| - \ln|x-\zeta_{4i-1}| - \ln|x-\zeta_{4i}| \right) + c(N) + d(N) \ln \rho \right], \quad (13)$$

where $c(N)$ and $d(N)$ are unknown coefficients which can be numerically determined by matching the inner and outer boundary conditions.

After matching the inner and outer boundary conditions, the numerical values of unknown $c(N)$ and $d(N)$ are determined as shown in Figs. 5-7, for fixed-fixed, fixed-free and free-fixed cases, respectively. It is found that all the numerical values in Figs. 5-7 match well with the analytical formulae of $c(N)$ and $d(N)$ in the Table 1 using the degenerate kernel.

3. Derivation of the Green's function for an annular case by using the Trefftz method

The problem of annular case can be decomposed into two parts. One is infinite plane with a concentrated source (fundamental solution) and the other is annular circles subject to specified boundary conditions as shown in Fig. 8. The first part solution can be obtained from the fundamental solution as follows:

$$G_F(x, \zeta) = \frac{\ln|x-\zeta|}{2\pi}. \quad (14)$$

The second part is solved by using the Trefftz method. The solution can be superposed by using the Trefftz base as shown below:

$$G_T(x, \zeta) = \sum_{j=1}^{N_T} c_j \Phi_j, \quad (15)$$

where Φ_j is the j^{th} T-complete function and N_T is the number of T-complete functions. Here, the T-complete functions are given as 1 , $\rho^m \cos m\phi$, $\rho^m \sin m\phi$ for the interior case and $\ln \rho$, $\rho^{-m} \cos m\phi$, $\rho^{-m} \sin m\phi$ for the exterior case. The complete bases for the annular problem can be represented by

$$G_T(x, \zeta) = p_0 + \bar{p}_0 \ln \rho + \sum_{m=1}^{\infty} \left[(p_m \rho^m + \bar{p}_m \rho^{-m}) \cos m\phi + (q_m \rho^m + \bar{q}_m \rho^{-m}) \sin m\phi \right], \quad (16)$$

where $x = (\rho, \phi)$, p_0 , \bar{p}_0 , p_m , \bar{p}_m , q_m and \bar{q}_m are unknown coefficients. By matching the boundary conditions, we substitute $x = (a, \phi)$ and $x = (b, \phi)$ in Eq. (15) to determine the unknown coefficients. Then, the series-form Green's functions are obtained in Table 1 for the three cases. For simplicity and without loss of generality, we prove the equivalence for the fixed-fixed case in the next section.

4. Mathematical equivalence between the solutions using the MFS and Trefftz method

4.1 Method of fundamental solutions (image method)

The image method can be seen as a special case of MFS, since its singularities are located outside the

domain. The Green's function of Eq. (12) can be expanded into series form by separating the field point $x(\rho, \phi)$ and source point $s(R, \theta)$ for the fundamental solution in the polar coordinate of Eq. (8) as shown below:

$$G(x, \zeta) = \frac{1}{2\pi} (\ln|x-\zeta| - \frac{\ln R_\zeta - \ln a}{\ln b - \ln a} \ln b - \frac{\ln b - \ln R_\zeta}{\ln b - \ln a} \ln \rho) + \frac{1}{2\pi} \sum_{i=1}^{\infty} \sum_{m=1}^{\infty} \frac{1}{m} \left[\left(\frac{\rho}{\zeta_{i-1}}\right)^m + \left(\frac{\zeta_i}{\rho}\right)^m - \left(\frac{\zeta_{i-2}}{\rho}\right)^m - \left(\frac{\rho}{\zeta_{i-3}}\right)^m \right] \cos m(\theta - \phi). \quad (17)$$

Without loss of generality, the source in the annular domain can be chosen as $\zeta = (R_\zeta, 0)$. By using Eqs. (4) and (5), all the images result in the four geometric series with the common ratio of a^2/b^2 which is smaller than one in Eq. (12) and can be rearranged into

$$G(x, \zeta) = \frac{\ln|x-\zeta|}{2\pi} + \frac{1}{2\pi} \sum_{m=1}^{\infty} \frac{1}{m} \left[\frac{R_\zeta^{2m} \rho^{2m} + a^{2m} b^{2m} - a^{2m} R_\zeta^{2m} - a^{2m} \rho^{2m}}{R_\zeta^m \rho^m (b^{2m} - a^{2m})} \right] \cos m\phi - \frac{1}{2\pi} \frac{\ln R_\zeta - \ln a}{\ln b - \ln a} \ln b - \frac{1}{2\pi} \frac{\ln b - \ln R_\zeta}{\ln b - \ln a} \ln \rho, \quad a \leq \rho \leq b, \quad (18)$$

after expanding all the image singularities. Regarding the optimal location for singularities of MFS, it is interesting to find that the optimal location may not be the expansion type of Fig. 9(a) or angular distribution of Fig. 9(b) but a lumped singularity in one radial direction as shown in Fig. 9(c). In this paper, our image location in the MFS only lumps on the radial direction which agrees with the optimal location found by Alves and Antunes [12].

4.2 Trefftz method

Since the angle of source can be set to zero without loss of generality, the coefficients in the Table 1 can be simplified. Then, the Green's function in Eq. (16) can be rewritten as

$$G(x, \zeta) = \frac{\ln|x-\zeta|}{2\pi} + \frac{1}{2\pi} \sum_{m=1}^{\infty} \frac{1}{m} \left[\frac{R_\zeta^{2m} \rho^{2m} + a^{2m} b^{2m} - a^{2m} R_\zeta^{2m} - a^{2m} \rho^{2m}}{R_\zeta^m \rho^m (b^{2m} - a^{2m})} \right] \cos m\phi - \frac{1}{2\pi} \frac{\ln R_\zeta - \ln a}{\ln b - \ln a} \ln b - \frac{1}{2\pi} \frac{\ln b - \ln R_\zeta}{\ln b - \ln a} \ln \rho, \quad a \leq \rho \leq b. \quad (19)$$

After comparing Eq. (18) with Eq. (19), it is found that the two solutions Eqs. (12) and (16) have been proved to be mathematically equivalent through the use of addition theorem, when the number of images and the number of Trefftz bases are both infinite. The equivalence of solution using the Trefftz method and MFS(image method) is summarized in Fig. 10. Similarly, the mathematical proof of the equivalence between Trefftz and MFS solutions can be extended to fixed-free and free-fixed cases without any difficulty. All the results are shown in Table 1.

5. Illustrative examples and discussions

For simplicity, an annular problem subject to the

Dirichlet boundary condition is considered here where the source is located at $\zeta = (7.5, 0)$. The two radii of inner and outer circles are 4 and 10, respectively. Although the Trefftz solution and MFS (image method) solution are proved to be mathematically equivalent in the infinite dimension ($N \rightarrow \infty$ and $N_T \rightarrow \infty$), they are not equivalent in the error analysis. The convergence rate under the finite number of degrees of freedoms is an interesting topic. Three approaches, (a) MFS with angular singularities, (b) MFS with images and (c) Trefftz method, are considered here. Their distributions of source and collocation points are shown in Fig. 11. The contour plots of analytic solutions using the Trefftz method and image method are shown in Figs. 12-14 for fixed-fixed, fixed-free and free-fixed cases, respectively. Figure 15 shows the potential at the point $(6, \pi/3)$ versus the number of terms by using various approaches. It is found that the convergence rate of image method is better than those of Trefftz method and conventional MFS. However, the results of Trefftz method are the worst. Fig. 16 shows the normal derivatives along outer and inner boundaries. The norm error of normal derivatives for outer and inner boundaries versus the number of terms ($N_T = M$) is shown in Fig. 17. Also, the results of the image method are better than those of the conventional MFS and the Trefftz method.

In this example, all the three figures (Figs. 15-17) indicate that the image method is more efficient than MFS with angular singularities and Trefftz method. The reason can be explained that source points in MFS were optimally selected by using the image concept. According to the addition theorem, the Trefftz bases are all imbedded in the degenerate kernel. Trefftz bases and $\ln r$ singularity are both complete for representing the solution. Although it is proved that the solution derived by using the image method and the Trefftz method are equivalent when the number of degrees of freedom is infinite. Nevertheless, their efficiencies are different on the finite number of degree of freedoms. Here, we find that the radial distribution of singularity is better than the angular distribution in the MFS. Also, we proved that the bases of MFS are more efficient than that of the Trefftz method in the fixed-fixed cases.

6. Concluding remarks

In this paper, not only the image method (a special case of MFS) but also the Trefftz method were employed to solve the Green's function of annular Laplace problem. Three cases, fixed-fixed, fixed-free and free-fixed were considered. The two solutions using the Trefftz method and MFS were proved to be mathematically equivalent by using addition theorem or so-called degenerate kernel. On the basis of finite number of degrees of freedoms, the results of image method are found to converge faster than those of Trefftz method and MFS with angular singularities. Also, the solution of image method shows the existence of the free constant which is always overlooked in the conventional MFS. Finally, we also found the final two frozen image points at the origin and

infinity where their strengths can be determined numerically and analytically in a consistent manner.

7. References

[1] E. Kita and N. Kamiya, "Trefftz method: an overview," *Adv. Engng. Softw.*, vol. 24, pp. 3-12, 1995.

[2] V.D. Kupradze and M.A. Aleksidze, "A method for the approximate solution of limiting problems in mathematical physics," *Computat. Math. Math. Phys.*, vol. 4, pp. 199-205, 1964.

[3] G. Fairweather and A. Karageorghis, "The method of fundamental solutions for elliptic boundary value problems," *Adv. Comput. Math.*, vol. 9, pp. 69-95, 1998.

[4] Y.A. Melnikov, "Some applications of the Green's function method in mechanics," *Int. J. Solids. Struct.*, vol. 13, pp. 1045-1058, 1977.

[5] W. Thomson "Maxwell in his treatise," *quotes a paper in the Cambridge and Dublin Math. Journal of 1848*, vol. I., Chap. XI, 1848.

[6] J.T. Chen and C.S. Wu, "Alternative derivations for the Poisson integral formula," *Int. J. Math. Educ. Sci. Technol.*, vol. 37, pp. 165-185, 2006.

[7] R. Courant and D. Hilbert, *Methods of mathematical physics*, New York, Interscience; 1953.

[8] A. Bogomolny, "Fundamental solutions method for elliptic boundary value problems," *SIAM J. Numer. Anal.*, vol. 22(4), pp. 644-669, 1985.

[9] Z.C. Li, T.T. Lu, H.Y. Hu and A.H.D. Cheng, *Trefftz and collocation methods*, Boston-Southampton, WIT Press; 2007.

[10] J.T. Chen, C.S. Wu, Y.T. Lee and K.H. Chen, "On the equivalence of the Trefftz method and method of fundamental solutions for Laplace and biharmonic equations," *Comp. Math. Appl.*, vol. 53, pp. 851-879, 2007.

[11] R. Shaback, *Adaptive Numerical Solution of MFS System*, ICCES Special Symposium on Meshless Methods, Cyprus; 2007.

[12] C.J.S. Alves and P.R.S. Antunes, "The method of fundamental solutions applied to the calculation of eigenfrequencies and eigenmodes of 2D simply connected shapes," *Comp. Mater. and Conti.*, vol. 2(4), pp. 251-265, 2005.

[13] J.T. Chen, Y.T. Lee, S.R. Yu and S.C. Shieh, "Equivalence between Trefftz method and method of fundamental solution for annular Green's function using the addition theorem and image concept," *Engng. Anal. Bound. Elem. Revised*, 2008.

[14] M.D. Greenberg, *Application of Green's functions in science and engineering*, Prentice-Hill, New Jersey; 1971.

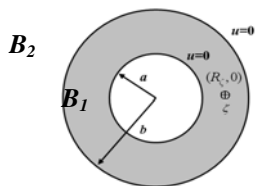


Fig. 1 Sketch of an annular problem subject to a concentrated load.

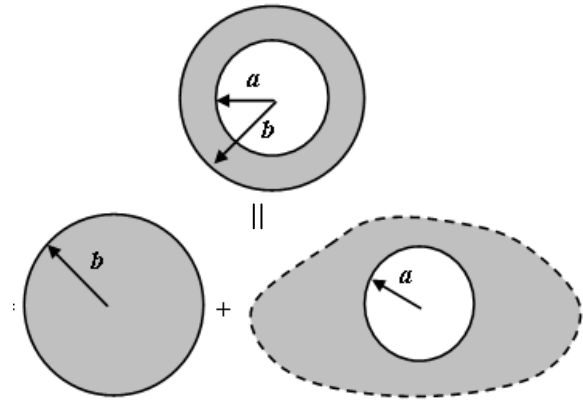


Fig. 2 An annular case composed of interior and exterior domains.

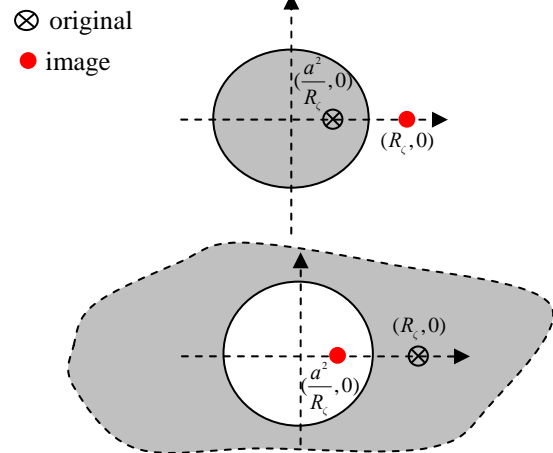


Fig. 3 Sketch of position of image point for the interior and exterior cases.

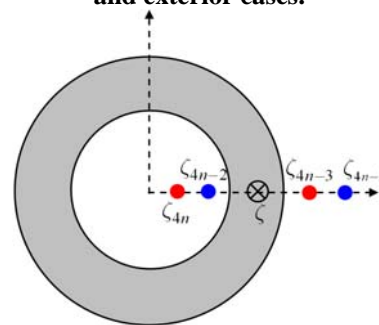


Fig. 4 The images for an annular problem.

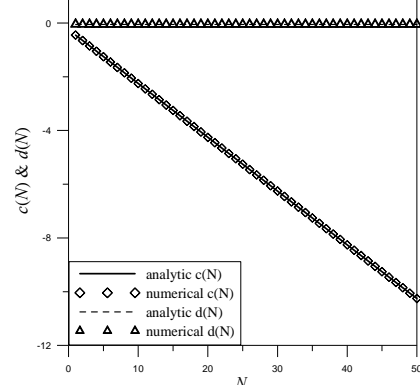


Fig. 5 Values of $c(N)$ and $d(N)$ for the fixed-fixed case.

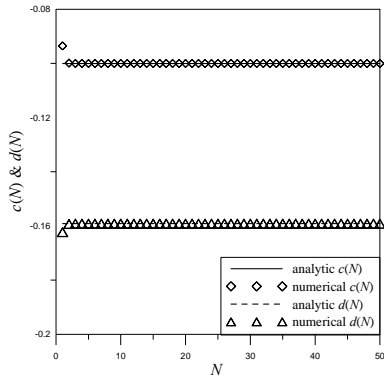


Fig. 6 Values of $c(N)$ and $d(N)$ for the fixed-free case.

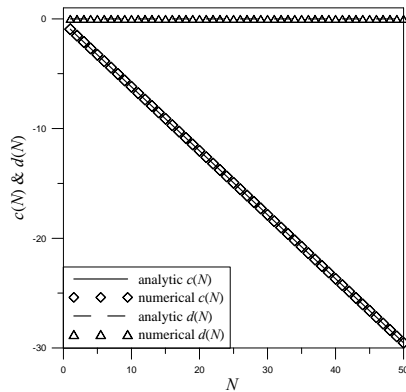


Fig. 7 Values of $c(N)$ and $d(N)$ for the free-fixed case.

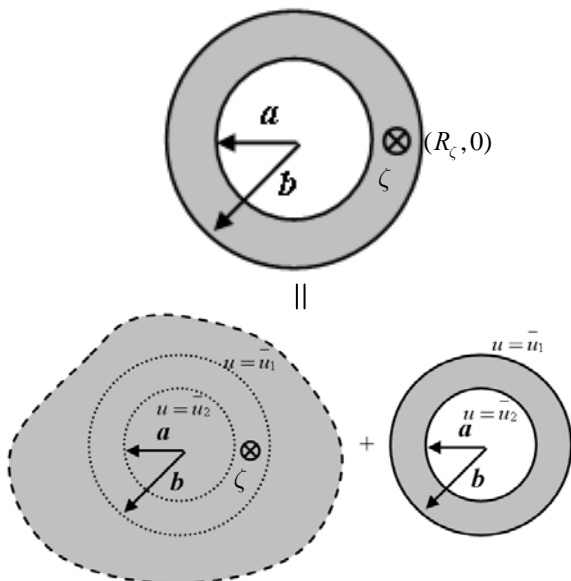


Fig. 8 Sketch of the superposition approach.

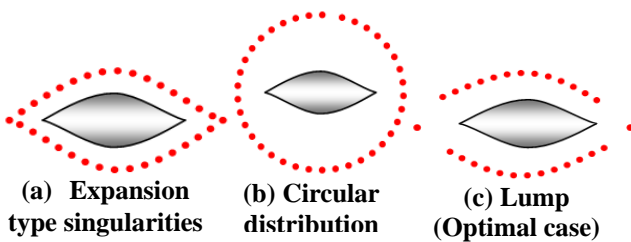


Fig. 9 Optimal locations for the MFS [11].

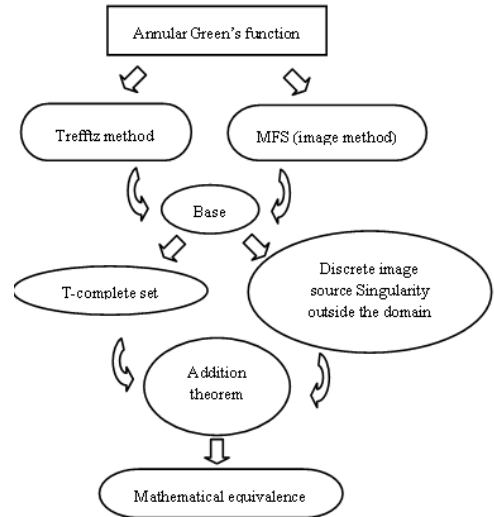
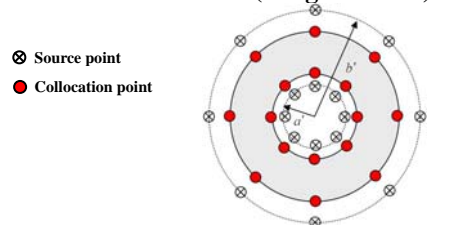
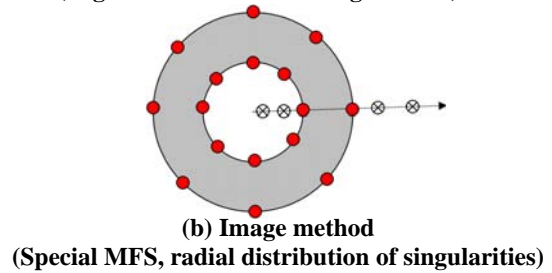


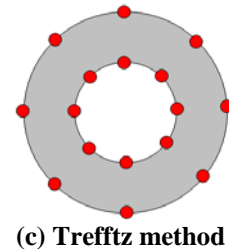
Fig. 10 Equivalence between the Trefftz method and MFS (image method).



(a) Conventional MFS (angular distribution of singularities)

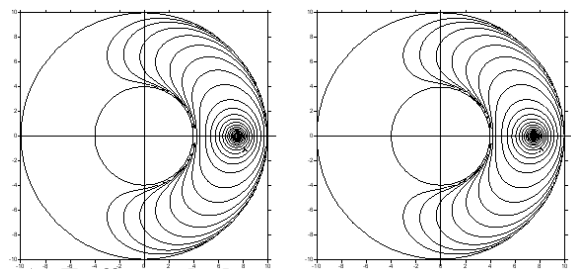


(b) Image method (Special MFS, radial distribution of singularities)



(c) Trefftz method

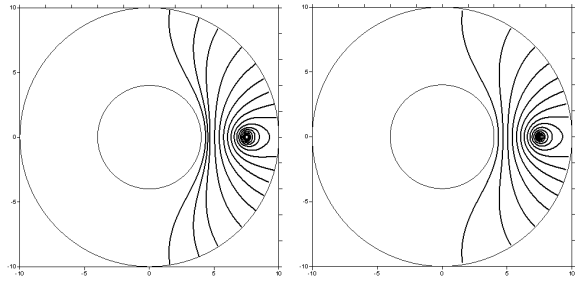
Fig. 11 Sketches of MFS, image method and Trefftz method.



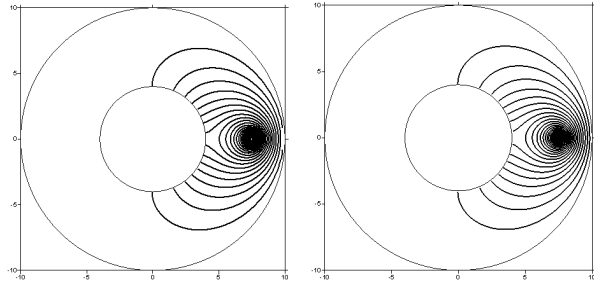
(a) Trefftz method

(b) Image method

Fig. 12 Contour plot for the analytical solution (fixed-fixed boundary condition).



(a) Trefftz method (b) Image method
Fig. 13 Contour plot for the analytical solution (fixed-free boundary condition).



(a) Trefftz method (b) Image method
Fig. 14 Contour plot for the analytical solution (free-fixed boundary condition).

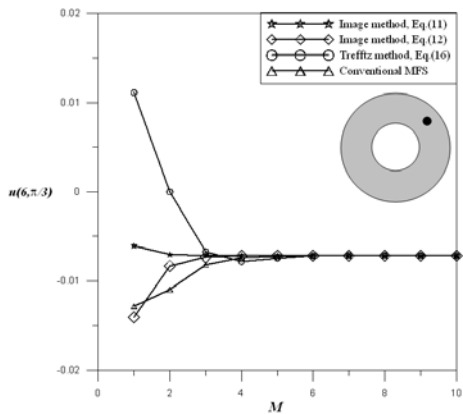
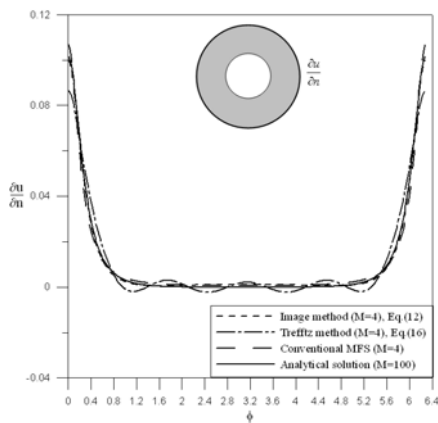
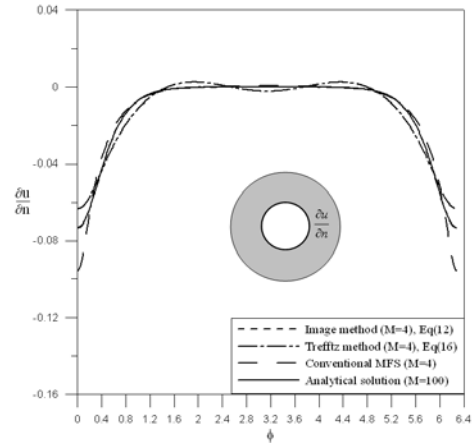


Fig. 15 Pointwise convergence test for the potential $u(6, \frac{\pi}{3})$ by using various approaches.

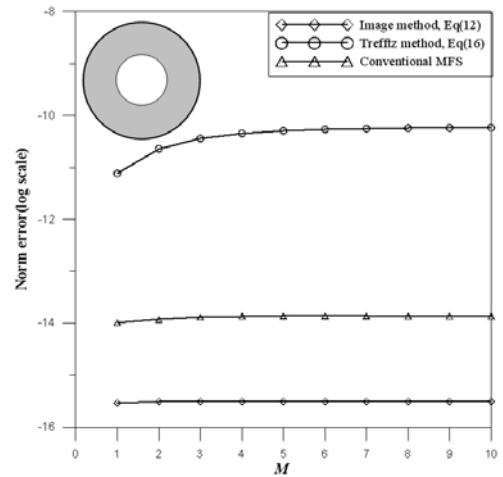


(a) Outer boundary

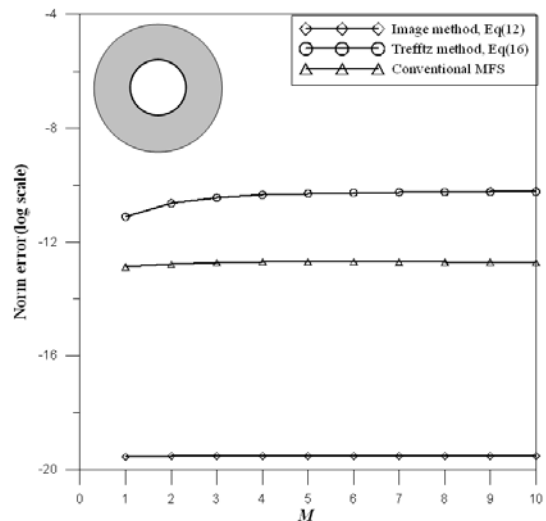


(b) Inner boundary

Fig. 16 Normal derivative along the inner and outer boundaries by using various approaches.



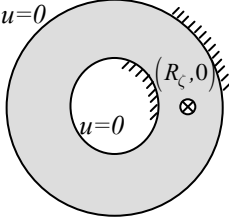
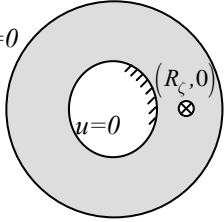
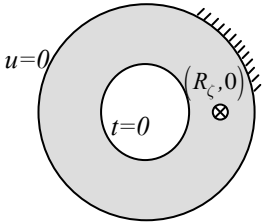
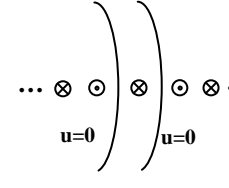
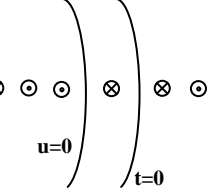
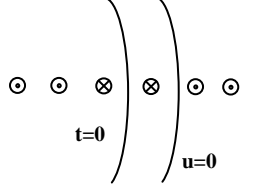
(a) Outer boundary



(b) Inner boundary

Fig. 17 L^2 norm error ($\int_0^{2\pi} |u(x) - \hat{u}(x)|^2 d\theta$) versus the number of terms.

Table 1 Trefftz and image solutions for fixed-fixed, fixed-free and free-fixed annular Green's functions.

| Boundary Method |  |  |  | | |
|--------------------|---|---|--|---|---|
| Trefftz solution | $G(x, \zeta) = \frac{\ln x-\zeta }{2\pi} + p_0 + \bar{p}_0 \ln \rho + \sum_{m=1}^{\infty} \left[p_m \rho^m \cos m\theta + q_m \rho^m \sin m\theta + \bar{p}_m \rho^{-m} \cos m\theta + \bar{q}_m \rho^{-m} \sin m\theta \right]$ | | | | |
| | $\begin{Bmatrix} p_0 \\ \bar{p}_0 \end{Bmatrix}$ | $\begin{Bmatrix} \frac{-\ln b (\ln a - \ln R_c)}{2\pi (\ln a - \ln b)} \\ -(\ln b - \ln R_c) \\ \frac{2\pi (\ln b - \ln a)}{2\pi (\ln b - \ln a)} \end{Bmatrix}$ | $\begin{Bmatrix} \frac{\ln a - \ln R_c}{2\pi} \\ -1 \\ \frac{2\pi}{2\pi} \end{Bmatrix}$ | $\begin{Bmatrix} -\frac{1}{2\pi} \ln b \\ 0 \end{Bmatrix}$ | |
| | $\begin{Bmatrix} p_m \\ \bar{p}_m \end{Bmatrix}$ | $\begin{Bmatrix} \frac{\cos m\theta \left[R_c^m - a^m \left(\frac{a}{R_c} \right)^m \right]}{2m\pi (b^{2m} - a^{2m})} \\ a^m b^m \cos m\theta \left[b^m \left(\frac{a}{R_c} \right)^m - a^m \left(\frac{R_c}{b} \right)^m \right] \\ 2m\pi (b^{2m} - a^{2m}) \end{Bmatrix}$ | $\begin{Bmatrix} \frac{\cos m\theta \left[a^m \left(\frac{a}{R_c} \right)^m - R_c^m \right]}{2m\pi (b^{2m} + a^{2m})} \\ a^m b^m \cos m\theta \left[b^m \left(\frac{a}{R_c} \right)^m + a^m \left(\frac{R_c}{b} \right)^m \right] \\ 2m\pi (b^{2m} + a^{2m}) \end{Bmatrix}$ | $\begin{Bmatrix} \frac{\cos m\theta \left[R_c^m + a^m \left(\frac{a}{R_c} \right)^m \right]}{2m\pi (b^{2m} + a^{2m})} \\ -a^m b^m \cos m\theta \left[b^m \left(\frac{a}{R_c} \right)^m - a^m \left(\frac{R_c}{b} \right)^m \right] \\ 2m\pi (b^{2m} + a^{2m}) \end{Bmatrix}$ | |
| | $\begin{Bmatrix} q_m \\ \bar{q}_m \end{Bmatrix}$ | $\begin{Bmatrix} \frac{a^m b^m \sin m\theta \left[b^m \left(\frac{a}{R_c} \right)^m - a^m \left(\frac{R_c}{b} \right)^m \right]}{2m\pi (b^{2m} - a^{2m})} \\ \sin m\theta \left[b^m \left(\frac{R_c}{b} \right)^m - a^m \left(\frac{a}{R_c} \right)^m \right] \\ 2m\pi (b^{2m} - a^{2m}) \end{Bmatrix}$ | $\begin{Bmatrix} \frac{\sin m\theta \left[a^m \left(\frac{a}{R_c} \right)^m - R_c^m \right]}{2m\pi (b^{2m} + a^{2m})} \\ a^m b^m \sin m\theta \left[b^m \left(\frac{a}{R_c} \right)^m + a^m \left(\frac{R_c}{b} \right)^m \right] \\ 2m\pi (b^{2m} + a^{2m}) \end{Bmatrix}$ | $\begin{Bmatrix} \frac{\sin m\theta \left[R_c^m + a^m \left(\frac{a}{R_c} \right)^m \right]}{2m\pi (b^{2m} + a^{2m})} \\ -a^m b^m \sin m\theta \left[b^m \left(\frac{a}{R_c} \right)^m - a^m \left(\frac{R_c}{b} \right)^m \right] \\ 2m\pi (b^{2m} + a^{2m}) \end{Bmatrix}$ | |
| Image solution |  | | |  |  |
| | $G(x, \zeta) = \frac{1}{2\pi} \left\{ \ln x-\zeta - \sum_{n=1}^N \left[\ln x-\zeta_{4n-3} + \ln x-\zeta_{4n-2} - \ln x-\zeta_{4n-1} - \ln x-\zeta_{4n} \right] - \left(2N \ln \frac{R_c}{a} + \ln b \frac{\ln a - \ln R_c}{\ln a - \ln b} - \frac{\ln b - \ln R_c}{(\ln b - \ln a)} \ln \rho \right) \right\}, \quad a \leq \rho \leq b$ | | | | |
| | $c(N)$ | $-\left(2N \ln \frac{R_c}{a} + \ln b \frac{\ln a - \ln R_c}{\ln a - \ln b} \right)$ | $\ln a - \ln R_c$ | $-(\ln b + 4N \ln \frac{b}{a})$ | |
| | $d(N)$ | $-\frac{\ln b - \ln R_c}{(\ln b - \ln a)}$ | -1 | 0 | |